Polarized sub-meV Photoluminescence in 2D PbS Nanoplatelets at Cryogenic Temperatures

Pengji Li[‡,1], Leon Biesterfeld[‡,2,3,5], Lars Klepzig[2,3], Jingzhong Yang[1], Huu Thoai Ngo[6], Ahmed Addad[7], Tom N. Rakow[1], Ruolin Guan[1], Eddy P. Rugeramigabo[1], Louis Biadala[,6], Jannika Lauth[*,2,3,4,5], Michael Zopf[*,1,4]*

[1]Institute of Solid State Physics, Leibniz University Hannover, Appelstraße 2, D-30167 Hannover, Germany.

[2]Cluster of Excellence PhoenixD (Photonics, Optics, and Engineering – Innovation Across Disciplines), Welfengarten 1A, D-30167 Hannover, Germany.

[3]Institute of Physical Chemistry and Electrochemistry, Leibniz University Hannover, Callinstr. 3A, D-30167 Hannover, Germany.

[4]Laboratory of Nano and Quantum Engineering, Leibniz University Hannover, Schneiderberg 39, D-30167 Hannover, Germany.

[5]Institute of Physical and Theoretical Chemistry, Eberhard Karls University of Tübingen, Auf der Morgenstelle 18, D-72076 Tübingen, Germany.

[6]Université de Lille, CNRS, Centrale Lille, Université Polytechnique Hauts-de-France, Junia-ISEN, UMR 8520 - IEMN, F-59000 Lille, France.

[7]Université Lille, CNRS, INRAE, Centrale Lille, UMR 8207 – UMET- Unité Matériaux et Transformations, F-59000 Lille, France

ABSTRACT

Colloidal semiconductor nanocrystals are promising materials for classical and quantum light sources due to

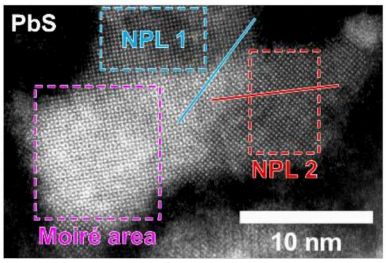

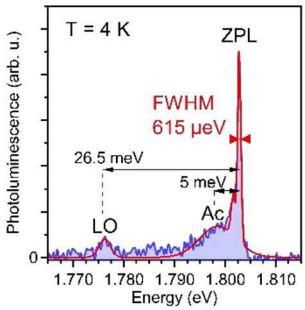

their versatile chemistry and efficient photoluminescence (PL) properties. While visible emitters are well-established, the pursuit of excellent (near-)infrared sources continues. One notable candidate in this regard are photoluminescent two-dimensional (2D) PbS nanoplatelets (NPLs) exhibiting excitonic emission at 720 nm (1.7 eV) directly tying to the typical emission range limit of CdSe NPLs. Here, we present the first comprehensive analysis of low-temperature PL from this material class. Ultrathin 2D PbS NPLs exhibit high crystallinity confirmed by scanning transmission electron microscopy, and revealing Moiré patterns in overlapping structures. At 4K, we observe unique PL features in single PbS NPLs, including narrow zero-phonon lines with line widths down to 0.6 meV and a linear degree of polarization up to 90%. Time-resolved measurements identify trions as the dominant emission source with a 2.3 ns decay time. Sub-meV spectral diffusion and no immanent blinking over minutes is observed, as well as discrete spectral jumps without memory effects. These findings advance the

understanding and underpin the potential of colloidal PbS NPLs for optical and quantum technologies.

Introduction

Colloidal semiconductor nanocrystals are being extensively studied for their use as classical and quantum light sources due to their optical properties dominated by size quantization.[1–3] Key requirements for their application include photo-stable PL with high quantum yields, fast radiative lifetimes, low spectral broadening and diffusion, as well as scalable fabrication. At UV to visible wavelengths, cadmium chalcogenide CdX (X = S, Se, and Te) NPLs and heterostructures are known for their excellent optical properties. In particular, CdSe-based NPL systems exhibit narrow linewidths below 40 meV at room temperature,[4,5] between 80 % and up to unity PL quantum yield,[6–8] fast radiative decay in the nanosecond range,[4,9] and highly directional PL.[10] In recent years, colloidal lead halide perovskite nanocrystals have emerged as emitters with efficient (quantum yield over 96%),[11] narrow (12 – 42 nm) and rapidly decaying (1 – 29 ns) room-temperature PL at visible wavelengths,[12] as well as single photon emission.[13–15] However, materials with similar characteristics at (near-) infrared (NIR) wavelengths are yet highly sought for, in particular for photonic quantum communication applications.[16–18] Potential candidates include Ag-doped CdSe NPLs,[19] HgTe NPLs[20] or InAs/CdSe core-shell nanocrystals.[21] Another promising material class are lead chalcogenide PbX (X = S, Se, Te) QDs[22–24], NPLs[25–27] and related heterostructures[28–30]: For instance, Krishnamurthy *et al.* demonstrated single spherical PbS/CdS QDs

emitting in the telecom O-band (near 0.95 eV) at room-temperature, featuring photon antibunching and an average line width of 89.5 meV.[29] In a similar system and at T = 4K, Hu *et al.* have reported on bleaching-free PL at around 1.0 eV and mean intrinsic PL line width of 16.4 meV, featuring asymmetric line shapes caused by the coupling of excitons to optical and acoustic phonon modes.[28] In both cases, the broad line widths (compared to their II-VI analogues, such as CdSe QDs) are a result of a 64-fold degenerated band-edge exciton in PbX QDs that splits into multiple energetically similar transitions, resulting in intrinsic PL broadening.[28,31,32] A closely related, yet unexplored system at the single particle level are photoluminescent 2D PbS NPLs. Manteiga Vázquez *et al.* developed a synthesis of rock salt cubic-structured PbS NPLs exhibiting a PL quantum yield of up to 19.4 % for PL at 1.7 eV (720 nm) upon surface passivation with $CdCl_2$.[25] This strongly enhanced emission efficiency provides the opportunity to investigate the excitonic emission properties of 2D PbS NPLs at the individual emitter level and exploring their electronic structure, phonon interactions and spectral characteristics at cryogenic temperatures.

Our findings provide the first in-depth optical study of individual PbS NPLs at cryogenic temperatures. Highly polarized emissions at around 1.82 eV (677.6 nm) with sub-meV linewidths are observed at T = 4K, accompanied by an acoustic phonon sideband. Time-resolved and excitation power dependent measurements reveal trion states as the dominant cause of PL. The emissions exhibit exceptional spectral stability with sub-meV spectral diffusion and are blinking-free over several minutes, promoting the potential of 2D PbS NPLs for reaching near-infrared optoelectronic applications.

Results and discussion

(NIR) emitting colloidal PbS NPLs were synthesized by a method described by Manteiga Vázquez *et al.*[25] Figure 1a shows a HR-HAADF-STEM image of two overlapping PbS NPLs; the corresponding FFT patterns of the highlighted crystal areas are depicted in Figure 1b-d. Individual PbS NPLs are highly crystalline and exhibit cubic rock salt structure (space group $Fm\bar{3}m$) expected for 2D PbS nanosheets (NSs) and NPLs[25,33,34] with the characteristic lattice spacings of 2.9 Å (200) and 2.1 Å (220) (PDF card 01-078-1900). Notably, no diffraction peaks of an orthorhombic PbS phase (interplane distances of 2.8 Å and 2.05 Å)[35] are evident from the FFT patterns in Figures 1b-d. The majority of NPLs resembles a rectangular shape with average lateral dimensions of (16.0 ± 1.6) x (9.2 ± 1.2) nm^2 and a corresponding aspect ratio of 1.7:1 (see Figure S1 for overview and corresponding size histogram). Strikingly, in the overlapping area, a Moiré pattern is formed as a result of the two differently oriented diffracting crystal lattices (see Figure S2 for additional examples). The apparent Moiré pattern is characteristic for a twist angle of 40°, which is in good agreement with the relative orientation of the two NPLs. In addition to the ultrathin 2D geometry combined with the highly crystalline nature of the synthesized structures, the presence of Moiré patterns indicates a ligand-free interface between single PbS NPLs. This unambiguously demonstrates that small $CdCl_2$ and metal halide ligands used for post-synthetic surface passivation in general, allow a quasi-direct contact between otherwise spatially separated NPLs (in contrast to bulky organic surfactants such as oleic acid), therefore bypassing the need for elaborate ligand removal processes.[26,36] Within such

Moiré lattices, the quantum confinement strongly depends on the twisting angle, thus serving as an additional tool for band gap engineering. While very thoroughly researched in the case of van der Waals materials,[37] twistronics based on other semiconductors (e.g. PbS) have only recently been accessed.[36]

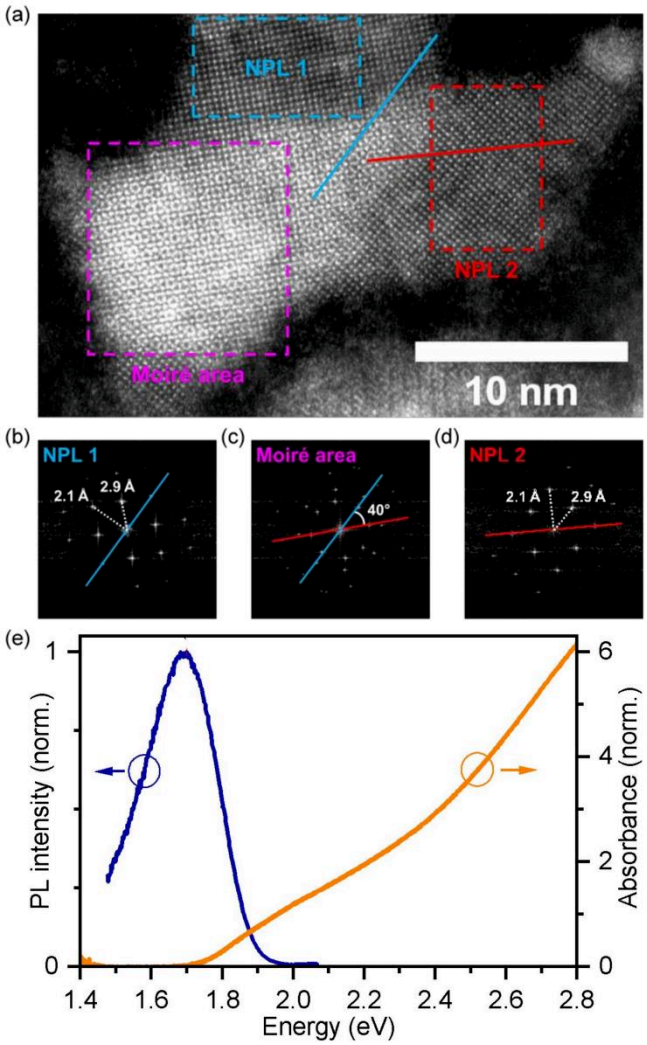

Figure 1. (a) HR-HAADF-STEM image of two overlapping PbS NPLs forming a Moiré pattern with a twist angle of 40°. The formation of the interference pattern underpins the ultrathin 2D geometry of the NPLs and indicates a ligand-free direct interface between the PbS NPLs. (b-d) Corresponding FFT patterns of the two NPLs and the Moiré area, substantiating the underlying cubic rock salt structure of the NPLs and the angle of 40°. (e) Ensemble room temperature absorbance and PL spectrum of PbS NPLs, exhibiting excitonic absorption at 1.96 eV and NIR PL at 1.70 eV.

The optical characteristics of the PbS NPLs at room-temperature comprise an excitonic absorption at 1.96 eV and associated NIR PL at 1.70 eV (Figure 1e) with a rather broad FWHM of 264 meV. To gain further insight into the optical, structural and electronic properties of PbS NPLs at the single NPL level, we apply cryogenic temperatures and perform PL measurements (see SI, section A).

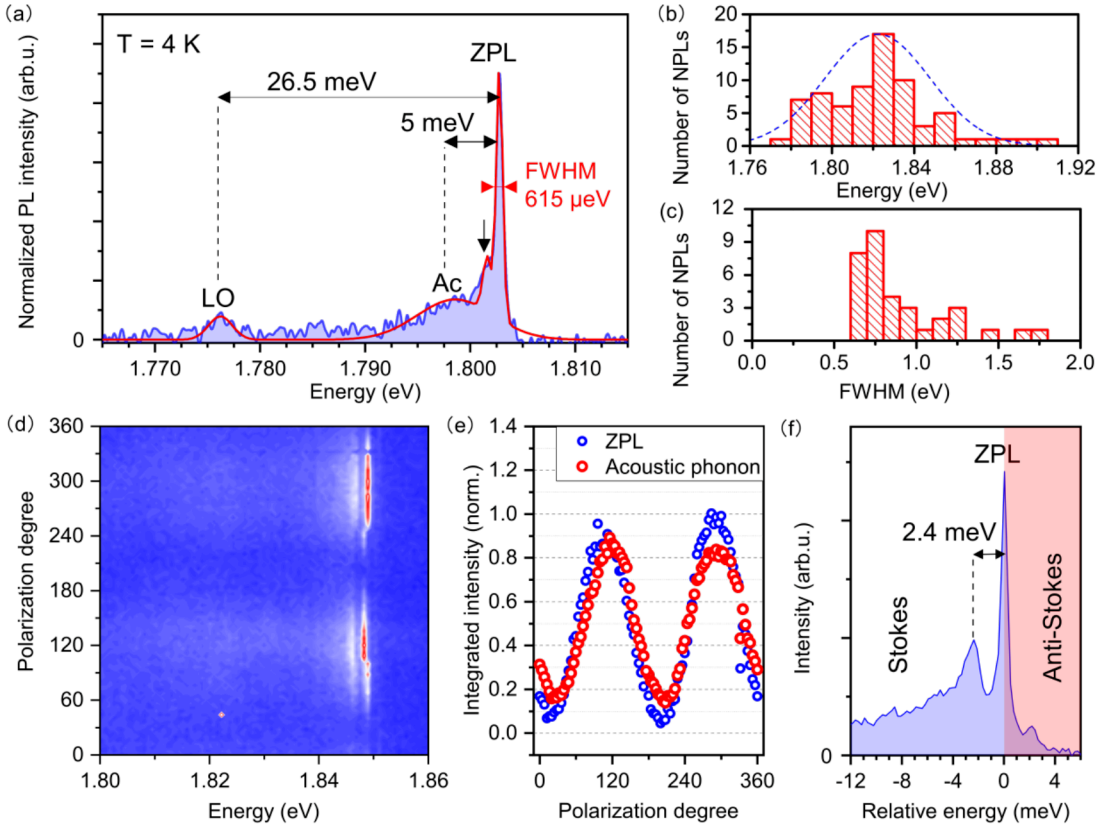

Figure 2. PL of single PbS NPLs at T = 4 K. (a) Micro-PL spectrum of a single PbS NPL (1s exposure time) featuring sub-meV emission and a red-shifted phonon sideband with LO-phonon replicas (LO) and acoustic phonon (Ac) contributions. (b) Distribution of the emission energy centered around 1.82 eV and (c) FWHM of the narrowband part of single PbS NPL emissions, obtained by measuring 71 individual NPLs. 74% of the measured emission lines exhibit sub-meV linewidths. (d) Polarization-dependent PL measurement of a single PbS NPL and (e) the respective normalized PL intensity obtained in different spectral ranges as a function of the linear polarization angle of the emitted light. The blue dots represent the ZPL ($\delta = 0.90$), the red dots correspond to the acoustic phonon sideband ($\delta = 0.71$). (f) Normalized sum of the 91 PL spectra from the measurement in (d) and illustration of Stokes and anti-Stokes PL of the acoustic phonon sidebands of a single PbS NPL.

Figure 2a shows a representative PL spectrum of individual PbS NPLs at T = 4K. In marked contrast with typical PL spectra of PbS nanocrystals for which single broad (≥ 8 meV) emission lines are observed, [28] the PL spectra of PbS NPLs consist of a narrow, resolution-limited, zero phonon line (ZPL) together with phonon sidebands at energies of 26.5 meV and 5 meV that we attribute to optical (LO) and acoustic phonons (Ac), respectively[28,38] (see Table S1 for the fitting results, Figures S4 and S5 for more spectra of individual NPLs). The statistics on more than 70 individual NPL show that the emission energies of the ZPL (Figures 2b) is centered around 1.82 ± 0.06 eV, which clearly indicates a high level of uniformity in the thickness and the lateral dimensions of the PbS NPLs. Moreover, Figure 2c shows that the NPL emission linewidth does not exceed 2 meV and more than 70% exhibit a resolution-limited linewidth (≤ 600 μeV FWHM). This strongly contrasts with the sharpest emission linewidth measured on individual PbS nanocrystals (≥ 8 meV) [28] for which the line broadening stems from the exciton fine structure, [28] the intervalley and the exciton-phonon coupling effects,[39] and the spectral diffusion.[40] Therefore, the record sharpness of the PbS NPLs studied here points to i) an absence of spectral diffusion, ii) a reduced exciton-phonon coupling and/or iii) a different excitonic origin of the emission. Strikingly, we observe an additional discrete peak (arrow in Figure 2a) close to the ZPL on the PL spectra. A detailed analysis of the PL spectra around the ZPL (conducted on another NPL, Figure 2f) unveils that this discrete peak appears in both, the Stokes and anti-Stokes part of the PL spectra. Such a well-defined peak observed around 2.4 meV for most of the NPLs is most likely stemming from the thickness breathing mode (which would be 2.4 meV

for a 1.6 nm thick PbS NPL. (see Figures S6 for TEM images of PbS NPLs exhibiting the thickness of 1-2 nm).[41,42] This feature, previously observed on PL spectra of individual CdSe[43] and InP[44] NCs at cryogenic temperatures, is the fingerprint of confined acoustic phonon modes at about 10K, which corresponds to the base temperature in cold-finger cryostats for such sample preparation.

Notwithstanding unprecedented sharpness of their emission lines, PbS NPLs exhibit striking linear polarization properties (Figure 2d), which are analyzed by utilizing a rotating half-wave plate followed by a polarizer. In Figure 2e, integrated intensities of the ZPL and the acoustic phonon sideband for the various polarization angles are reported. From the angle dependent PL intensity, we evaluate the polarization degree, δ, as $\delta = (I_{max}-I_{min})/(I_{max}+I_{min})$ where I_{max} (I_{min}) are the maximum (minimum) PL intensities. The ZPL displays a high polarization degree $\delta = 0.90$ (for similar data from a second PbS NPL, we refer to Figure S7). The acoustic phonon sideband (from -1 meV to -8 meV in Figure 2f) shows a slightly lower polarization degree of $\delta = 0.71$, while maintaining the same polarization angle as the ZPL.

The emission polarization of single NPLs is influenced by their aspect ratio,[31] as well as the orientation of the NPL with respect to the substrate. A dipole orientation in the plane of the substrate will show maximum polarization degree, whereas dipoles with orthogonal orientations are expected to appear as un-polarized emission (details in the SI, section B). The high degree of linear polarization in PbS NPLs indicates that the excitonic transition in individual PbS NPLs exhibits a polarization component, attributed to a linear 1D or 2D dipole. Furthermore, the alignment of the dipole is nearly

ideal to the substrate plane (similar to observations shown in Figure 1). The aspect ratio is PbS NPLs is approx. 2, leading to anisotropic lateral electronic confinement and therefore contributing to the enhanced degree of observed polarization. It is important to note that the degree of polarization may depend on further factors that we do not study in detail here, such as selection rules of the allowed excitonic states and the respective oscillator strengths or possible effects of absorption polarization, by which the recombination of specific exciton types can be favored depending on the excitation energy and the energy spectrum of the NPL.

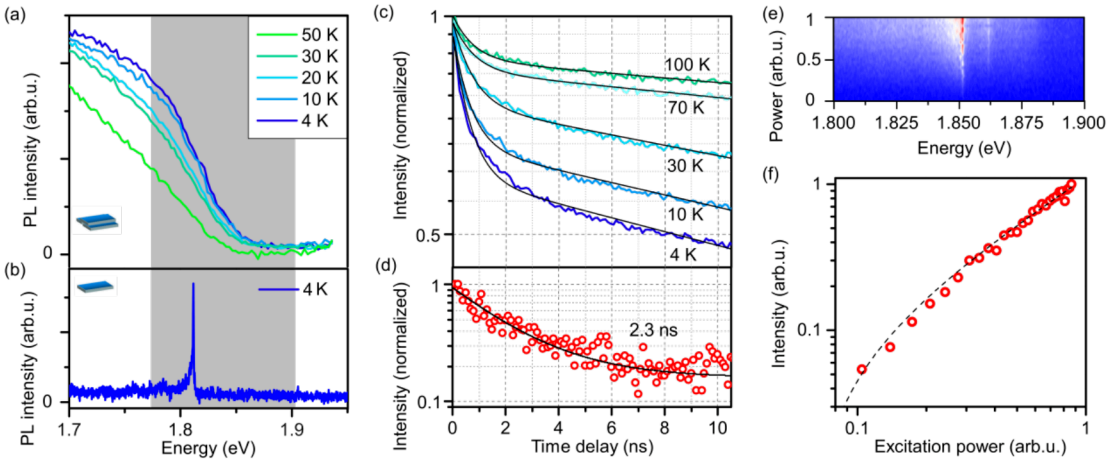

Figure 3. (a) Temperature-dependent, normalized PL spectra of an ensemble of PbS NPLs and (b) PL spectrum of a single PbS NPLs at 4 K. The gray shaded area indicates the spectral range selected for lifetime measurements. (c) Fluorescence lifetime measurements of an ensemble of PbS NPLs. Bi-exponential decay model (solid, black lines). (d) PL lifetime measurements of a single PbS NPL. A mono-exponential decay model is applied (solid, black line). (e) Excitation laser power dependent PL spectra from a single PbS NPL and (f) the respective normalized integrated PL intensity of ZPL showing a linear increase with the excitation power.

Figure 3 shows the comparison of PbS NPL ensemble with single NPL PL to study the origin and excitonic nature of the emission in more detail. Figure 3a includes the temperature-dependent, normalized PL spectra of a PbS NPL ensemble. We find an increasing slope of the high-energy PL edge with decreasing temperature, indicating an

increased relative intensity and a decreased spectral width of the bandgap-associated emission. The PL spectrum of a single NPL at 4 K in Figure 3b, as well as the distribution of emission energies discussed in Figure. 2b, shows good overlap with the emission edge of the ensemble emission at T = 4 K in Figure 3a.

The spectral region of the emission is then filtered (shaded gray area in Figure 3a, b) and detected with an avalanche photodiode to perform PL decay measurements for temperatures from 4 K to 100 K (Figure 3c). The decay dynamics occur on two markedly different timescales with a slow component τ_1 ($\geq$ 100 ns), weakly affected by the temperature and a fast (sub-ns) decay $\tau_{2,}$ with a vanishing amplitude as the temperature is increased (see Table S2). These dynamics stand compared to the PL decay of PbS nanocrystals, which typically occurs on a microsecond timescale (see Figure S8 for PL lifetime measurement of ensemble PbS NPLs at RT).[45,46] We attribute the presence of the fast component to the high repetition rate of the pulsed laser of 82 MHz, which favors the generation of higher order excitonic complexes (such as trions) by a pile-up effect. The vanishing of the fast component could be explained by the thermal energy overcoming the binding energy of the excitonic complex.

The PL decay of a single PbS NPL at 4 K is shown in Figure 3d, and data is best modelled with a mono-exponential decay, even though it cannot be ruled out completely that a smaller fraction with a slower decay component is present also in this case. A lifetime of 2.3 ns is extracted, which is in the realm of lifetimes reported for CdSe[47] and InP[48] NCs.

A further tool to investigate the excitonic origin of NPLs and nanocrystals are excitation power dependent measurements.[49,50] We perform these measurements under CW excitation with results shown in Figure 3e. A linear increase of the integrated PL intensity of the ZPL (Figure 3f) and the lack of additional spectral features with growing excitation power rules out multi-excitonic emissions as well as recombination processes that are independent of the excitation power (such as those involving trap or defect states).

By considering all observations up to this point, the question arises whether the narrow-band emission in single PbS NPLs can either be attributed to the presence of neutral excitons or trions, i.e. an exciton in presence of an additional unpaired charge carrier. Owing to their specific spin structure,[51] optical properties of trions (positive and negative) include rather temperature-independent emission characteristics.[52] This results in trion emission having a rapid initial decay phase, which is indicative of swift radiative recombination. This phase is faster than the decay of dark excitons, yet slower than that of bright excitons.[52] The unique dynamics of neutral excitons, which are susceptible to temperature due to the interplay between optically inactive (dark) and active (bright) states, are in stark contrast with the more temperature-stable behavior of trions. However, the proportion of trion transitions is sensitive to temperature, particularly in relation to their binding energy. When thermal energy surpasses the trion binding energy, the trion emission effectively vanishes. This aligns well with observations from the PbS NPL ensemble PL decay as a function of temperature, which demonstrates that, while the rate of fast PL decay remains constant, its relative weight

diminishes with an increase in temperature. Based on these factors, we assume the fast decay of the narrowband emission of single PbS NPLs at 4 K is initiated by a trion transition. The sign of the trion does not affect the conclusion but further studies on the magneto-optical properties of the trion will aim at unveiling the sign of the trion and their spin dynamics.

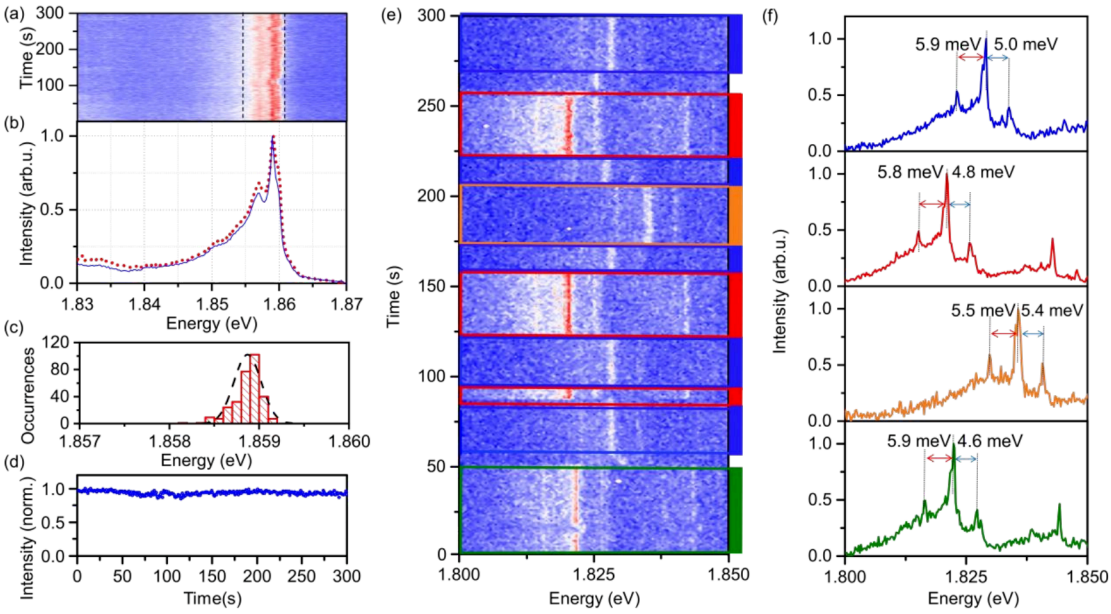

Figure 4. Spectral and temporal dynamics of single PbS NPLs. (a) PL time traces of a representative PbS nanoplatelet, exhibiting minimal spectral diffusion and blinking. (b) Normalized sum (red, dashed line) of the 300 PL spectra from (a). The blue line features the normalized sum of spectra which is corrected for spectral diffusion by rescaling the x-axis of each spectrum to the emission energy of the strongest emission peak. (c) Distribution of the central emission energy of the emission (obtained by fitting each spectrum in (a)) and (d) intensity time trace from the emission in (a) within the integration range shown by the dashed line. (e) PL time trace of a single PbS NPLs, revealing combined spectral diffusion and blinking with discrete jumps. (f) Normalized sum of spectra for the four distinct emission states observed in (e), with the spectrum's color corresponding to the selected ranges in (e).

To characterize the spectro-temporal dynamics in PbS NPLs, we analyze PL time traces of individual NPLs at a cryostat temperature of 4 K. These dynamics are key to understanding the influence of the nanomaterials' surroundings on their photophysical

properties. Figure 4a shows 300 consecutively recorded spectra with 1 s exposure time each, exhibiting a highly stable emission of PbS NPLs. All recorded spectra are summed up and normalized to obtain a time-integrated spectrum over 300 s (dashed red line in Figure 4b). A second approach addresses the spectral diffusion by rescaling the x-axis of each individual spectrum to match the emission energy of the strongest emission peak, followed by summing up these adjusted spectra and normalizing them (solid blue line in Figure 4b). The excellent overlap between the normalized sum of spectra and the spectral diffusion-compensated normalized sum of spectra underpins that the effect of spectral diffusion in the single PbS NPL emission is almost negligible over 5 min (see Figure S9 and S10 for more timetrace measurements of individual PbS NPLs). The distribution of the central emission energy, derived from applying a Gaussian line shape to each spectrum, is presented in Figure 4c and reveals sub-meV (FWHM of 0.4 meV) spectral diffusion. The reduced fast spectral dynamics, which typically occurs due to the Stark effect induced by trapped surface charges, points to a low density of surface traps. The application of $CdCl_2$ in a post-synthetic step for surface passivation has been identified as an effective strategy for addressing undersaturated surface atoms *via* X- and Z-type binding to Pb^{2+} and S^{2-} ions, respectively, and contributes to a reduced trap state density.[25,26] Mid-gap trap states are also expected to be of low level of significance due to the high crystallinity and well-balanced stoichiometry (Figure 1 and also Manteiga *et. al.*[20]), as well as an expected robustness of PbS NPLs against off-stoichiometry predicted in *ab-initio* simulations.[53] Figure 4d shows the time-dependent intensity of the emitted signal shown in Figure 4a,

within the spectral region indicated with dashed lines. A stable emission is observed over long times with no clear traces of blinking and only slow, low-magnitude drifts of the intensity, which is yet another argument for a low trap-state density in PbS NPLs.

While the low spectral diffusion is a common feature of the studied NPLs, the spectral characteristics can vary considerably. Figure 4e illustrates the spectral evolution of another PbS NPL, which displays several discrete spectral jumps over time. Four distinct spectral positions were identified, and for each of these we show the normalized sum of the respective spectra in Figure 4f by using the same color. Despite the differences in spectral position, the spectra are almost identical: The ZPL as well as observed Stokes and anti-Stokes PL features with phonon energies of around 5-6 meV do not change significantly. Another noteworthy feature is the lack of memory effect[54] at the spectral jumps, which indicates that the spectral positions correspond to discrete localized states that are not correlated or affected by the previous state of the NPL. These observations could be consistent with a trion emission experiencing four different Coulomb environments (e.g., four localized trapping sites) where the spectral positions are determined by the quantum-confined Stark effect induced by a charge carrier trapping. The absence of spectral diffusion (see Figure S11) at each spectral position indicates that the charges remain strongly localized as hopping charges would cause Stark effect fluctuations.

Conclusion

In conclusion, we have synthesized highly crystalline, ultrathin 2D PbS NPLs with $CdCl_2$ ligands used for surface passivation. A comprehensive analysis of the PL

properties of these PbS NPLs is conducted at cryogenic temperatures. The results reveal that single PbS NPLs exhibit strong and linearly polarized emission at 4 K, showcasing sub-meV linewidths significantly narrower than those observed in spherical nanocrystals of similar materials. These findings highlight the unique optical properties conferred by the 2D geometry of the PbS NPLs. Time-resolved PL measurements confirm that the narrow emission originate from trions. The trion state in PbS NPLs demonstrates stable emission with minimal spectral diffusion and the absence of blinking over minutes. Additionally, PbS NPLs exhibit new spectral diffusion characteristics, which lack a memory effect. Our findings not only advance the fundamental understanding of colloidal 2D semiconductor NPLs but also emphasize their significant potential for advancing the next generation of optical and quantum technologies.

AUTHOR INFORMATION

Corresponding Authors

*E-mail: michael.zopf@fkp.uni-hannover.de

*E-mail: jannika.lauth@uni-tuebingen.de

*E-mail: louis.biadala@iemn.fr

Author Contributions

J.L. and M.Z. conceived the project and supervised the experiments. Optical measurements were conducted by P.L (low-temperature) and L.K. (room-temperature).

The low-temperature measurements were supported by J.Y. and the respective data analysis by T.N.R. H.T.N. and A.A. performed the TEM experiments under the supervision of L.B. L.B., J.L and M.Z. contributed strongly to the interpretation of the data. P.L. and E.P.R. prepared the samples for Low temperature micro-PL. P.L. and R.G. performed the polarization simulation. The manuscript was written by P.L. and L.B., with input from all co-authors.

‡ These authors contributed equally.

Notes

The authors declare no competing financial interest.

ACKNOWLEDGMENT

The authors gratefully acknowledge the German Federal Ministry of Education and Research (BMBF) within the projects SemIQON (13N16291) and QVLS-iLabs: Dip-QT (03ZU1209DD), as well as the Deutsche Forschungsgemeinschaft (DFG, German Research Foundation) under Germany's Excellence Strategy (EXC-2123) Quantum Frontiers (390837967). P. Li acknowledges the China Scholarship Council (CSC201807040076). L. B., L. F. K. and J. L. gratefully acknowledge funding by the Deutsche Forschungsgemeinschaft (DFG, German Research Foundation) under Germany's Excellence Strategy within the Cluster of Excellence PhoenixD (EXC 2122, Project ID 390833453). J. L. is thankful for additional funding by an Athene Grant of the University of Tübingen (by the Federal Ministry of Education and Research (BMBF)

and the Baden-Württemberg Ministry of Science as part of the Excellence Strategy of the German Federal and State Governments).

The authors gratefully acknowledge Serguei Goupalov for fruitful discussions and Fei Ding for his strong support in the supervision and discussion of the experimental works.

REFERENCES

(1) Kagan, C. R.; Bassett, L. C.; Murray, C. B.; Thompson, S. M. Colloidal Quantum Dots as Platforms for Quantum Information Science. *Chem. Rev.* **2021**, *121* (5), 3186–3233.
(2) Pietryga, J. M.; Park, Y.-S.; Lim, J.; Fidler, A. F.; Bae, W. K.; Brovelli, S.; Klimov, V. I. Spectroscopic and Device Aspects of Nanocrystal Quantum Dots. *Chem. Rev.* **2016**, *116* (18), 10513–10622.
(3) Diroll, B. T.; Guzelturk, B.; Po, H.; Dabard, C.; Fu, N.; Makke, L.; Lhuillier, E.; Ithurria, S. 2D II–VI Semiconductor Nanoplatelets: From Material Synthesis to Optoelectronic Integration. *Chem. Rev.* **2023**, *123* (7), 3543–3624.
(4) Ithurria, S.; Tessier, M. D.; Mahler, B.; Lobo, R. P. S. M.; Dubertret, B.; Efros, Al. L. Colloidal Nanoplatelets with Two-Dimensional Electronic Structure. *Nature Mater* **2011**, *10* (12), 936–941.
(5) Ithurria, S.; Dubertret, B. Quasi 2D Colloidal CdSe Platelets with Thicknesses Controlled at the Atomic Level. *J. Am. Chem. Soc.* **2008**, *130* (49), 16504–16505.
(6) Schlosser, A.; Graf, R. T.; Bigall, N. C. CdS Crown Growth on CdSe Nanoplatelets: Core Shape Matters. *Nanoscale Adv.* **2020**, *2* (10), 4604–4614.
(7) Hu, A.; Bai, P.; Zhu, Y.; Song, Z.; Wang, R.; Zheng, J.; Yao, Y.; Zhang, Q.; Ding, Z.; Gao, P.; Sui, X.; Liu, X.; Gao, Y. Green CdSe/CdSeS Core/Alloyed-Crown Nanoplatelets Achieve Unity Photoluminescence Quantum Yield over a Broad Emission Range. *Advanced Optical Materials* **2022**, *10* (13), 2200469.
(8) Tessier, M. D.; Mahler, B.; Nadal, B.; Heuclin, H.; Pedetti, S.; Dubertret, B. Spectroscopy of Colloidal Semiconductor Core/Shell Nanoplatelets with High Quantum Yield. *Nano Lett.* **2013**, *13* (7), 3321–3328.
(9) Tessier, M. D.; Javaux, C.; Maksimovic, I.; Loriette, V.; Dubertret, B. Spectroscopy of Single CdSe Nanoplatelets. *ACS Nano* **2012**, *6* (8), 6751–6758.
(10) Scott, R.; Heckmann, J.; Prudnikau, A. V.; Antanovich, A.; Mikhailov, A.; Owschimikow, N.; Artemyev, M.; Climente, J. I.; Woggon, U.; Grosse, N. B.; Achtstein, A. W. Directed Emission of CdSe Nanoplatelets Originating from Strongly Anisotropic 2D Electronic Structure. *Nature Nanotech* **2017**, *12* (12), 1155–1160.
(11) Morad, V.; Stelmakh, A.; Svyrydenko, M.; Feld, L. G.; Boehme, S. C.; Aebli, M.;

Affolter, J.; Kaul, C. J.; Schrenker, N. J.; Bals, S.; Sahin, Y.; Dirin, D. N.; Cherniukh, I.; Raino, G.; Baumketner, A.; Kovalenko, M. V. Designer Phospholipid Capping Ligands for Soft Metal Halide Nanocrystals. *Nature* **2024**, *626* (7999), 542–548.
(12) Protesescu, L.; Yakunin, S.; Bodnarchuk, M. I.; Krieg, F.; Caputo, R.; Hendon, C. H.; Yang, R. X.; Walsh, A.; Kovalenko, M. V. Nanocrystals of Cesium Lead Halide Perovskites ($CsPbX_3$, X = Cl, Br, and I): Novel Optoelectronic Materials Showing Bright Emission with Wide Color Gamut. *Nano Lett.* **2015**, *15* (6), 3692–3696.
(13) Park, Y.-S.; Guo, S.; Makarov, N. S.; Klimov, V. I. Room Temperature Single-Photon Emission from Individual Perovskite Quantum Dots. *ACS Nano* **2015**, *9* (10), 10386–10393.
(14) Hu, F.; Zhang, H.; Sun, C.; Yin, C.; Lv, B.; Zhang, C.; Yu, W. W.; Wang, X.; Zhang, Y.; Xiao, M. Superior Optical Properties of Perovskite Nanocrystals as Single Photon Emitters. *ACS Nano* **2015**, *9* (12), 12410–12416.
(15) Rainò, G.; Nedelcu, G.; Protesescu, L.; Bodnarchuk, M. I.; Kovalenko, M. V.; Mahrt, R. F.; Stöferle, T. Single Cesium Lead Halide Perovskite Nanocrystals at Low Temperature: Fast Single-Photon Emission, Reduced Blinking, and Exciton Fine Structure. *ACS Nano* **2016**, *10* (2), 2485–2490.
(16) Cao, X.; Zopf, M.; Ding, F. Telecom Wavelength Single Photon Sources. *J. Semicond.* **2019**, *40* (7), 071901.
(17) Miyazawa, T.; Takemoto, K.; Sakuma, Y.; Hirose, S.; Usuki, T.; Yokoyama, N.; Takatsu, M.; Arakawa, Y. Single-Photon Generation in the 1.55-Mm Optical-Fiber Band from an InAs/InP Quantum Dot. *Jpn. J. Appl. Phys.* **2005**, *44* (5L), L620.
(18) Ward, M. B.; Karimov, O. Z.; Unitt, D. C.; Yuan, Z. L.; See, P.; Gevaux, D. G.; Shields, A. J.; Atkinson, P.; Ritchie, D. A. On-Demand Single-Photon Source for 1.3μm Telecom Fiber. *Applied Physics Letters* **2005**, *86* (20), 201111.
(19) Khan, A. H.; Pinchetti, V.; Tanghe, I.; Dang, Z.; Martín-García, B.; Hens, Z.; Van Thourhout, D.; Geiregat, P.; Brovelli, S.; Moreels, I. Tunable and Efficient Red to Near-Infrared Photoluminescence by Synergistic Exploitation of Core and Surface Silver Doping of CdSe Nanoplatelets. *Chem. Mater.* **2019**, *31* (4), 1450–1459.
(20) Izquierdo, E.; Robin, A.; Keuleyan, S.; Lequeux, N.; Lhuillier, E.; Ithurria, S. Strongly Confined HgTe 2D Nanoplatelets as Narrow Near-Infrared Emitters. *J. Am. Chem. Soc.* **2016**, *138* (33), 10496–10501.
(21) Xie, R.; Peng, X. Synthetic Scheme for High-Quality InAs Nanocrystals Based on Self-Focusing and One-Pot Synthesis of InAs-Based Core–Shell Nanocrystals. *Angew Chem Int Ed* **2008**, *47* (40), 7677–7680.
(22) Moreels, I.; Justo, Y.; De Geyter, B.; Haustraete, K.; Martins, J. C.; Hens, Z. Size-Tunable, Bright, and Stable PbS Quantum Dots: A Surface Chemistry Study. *ACS Nano* **2011**, *5* (3), 2004–2012..
(23) Murphy, J. E.; Beard, M. C.; Norman, A. G.; Ahrenkiel, S. P.; Johnson, J. C.; Yu, P.; Mićić, O. I.; Ellingson, R. J.; Nozik, A. J. PbTe Colloidal Nanocrystals: Synthesis, Characterization, and Multiple Exciton Generation. *J. Am. Chem. Soc.* **2006**, *128* (10), 3241–3247.
(24) Pietryga, J. M.; Schaller, R. D.; Werder, D.; Stewart, M. H.; Klimov, V. I.; Hollingsworth, J. A. Pushing the Band Gap Envelope: Mid-Infrared Emitting Colloidal

PbSe Quantum Dots. *J. Am. Chem. Soc.* **2004**, *126* (38), 11752–11753.
(25) Manteiga Vázquez, F.; Yu, Q.; Klepzig, L. F.; Siebbeles, L. D. A.; Crisp, R. W.; Lauth, J. Probing Excitons in Ultrathin PbS Nanoplatelets with Enhanced Near-Infrared Emission. *The Journal of Physical Chemistry Letters* **2021**, *12* (1), 680–685.
(26) Biesterfeld, L.; Klepzig, L. F.; Niebur, A.; Rosebrock, M.; Lauth, J. Toward Bright Colloidal Near-Infrared Emitters: Surface Passivation of 2D PbSe Nanoplatelets by Metal Halides. *J. Phys. Chem. C* **2022**, *126* (45), 19277–19285.
(27) Klepzig, L. F.; Biesterfeld, L.; Romain, M.; Niebur, A.; Schlosser, A.; Hübner, J.; Lauth, J. Colloidal 2D PbSe Nanoplatelets with Efficient Emission Reaching the Telecom O-, E- and S-Band. *Nanoscale Adv.* **2022**, *4* (2), 590–599.
(28) Hu, Z.; Kim, Y.; Krishnamurthy, S.; Avdeev, I. D.; Nestoklon, M. O.; Singh, A.; Malko, A. V.; Goupalov, S. V.; Hollingsworth, J. A.; Htoon, H. Intrinsic Exciton Photophysics of PbS Quantum Dots Revealed by Low-Temperature Single Nanocrystal Spectroscopy. *Nano Lett.* **2019**, *19* (12), 8519–8525.
(29) Krishnamurthy, S.; Singh, A.; Hu, Z.; Blake, A. V.; Kim, Y.; Singh, A.; Dolgopolova, E. A.; Williams, D. J.; Piryatinski, A.; Malko, A. V.; Htoon, H.; Sykora, M.; Hollingsworth, J. A. PbS/CdS Quantum Dot Room-Temperature Single-Emitter Spectroscopy Reaches the Telecom O and S Bands via an Engineered Stability. *ACS Nano* **2021**, *15* (1), 575–587.
(30) Correa, R. E.; Dauler, E. A.; Nair, G.; Pan, S. H.; Rosenberg, D.; Kerman, A. J.; Molnar, R. J.; Hu, X.; Marsili, F.; Anant, V.; Berggren, K. K.; Bawendi, M. G. Single Photon Counting from Individual Nanocrystals in the Infrared. *Nano Lett.* **2012**, *12* (6), 2953–2958.
(31) Nestoklon, M.; Avdeev, I. D.; Goupalov, S. V. Theory of Excitonic States in Lead Salt Quantum Dots. In *Quantum Sensing and Nano Electronics and Photonics XVII*; Razeghi, M., Lewis, J. S., Khodaparast, G. A., Khalili, P., Eds.; SPIE: San Francisco, United States, 2020; p 30.
(32) Kang, I.; Wise, F. W. Electronic Structure and Optical Properties of PbS and PbSe Quantum Dots. *J. Opt. Soc. Am. B* **1997**, *14* (7), 1632.
(33) Schliehe, C.; Juarez, B. H.; Pelletier, M.; Jander, S.; Greshnykh, D.; Nagel, M.; Meyer, A.; Foerster, S.; Kornowski, A.; Klinke, C.; Weller, H. Ultrathin PbS Sheets by Two-Dimensional Oriented Attachment. *Science* **2010**, *329* (5991), 550–553.
(34) Bielewicz, T.; Dogan, S.; Klinke, C. Tailoring the Height of Ultrathin PbS Nanosheets and Their Application as Field-Effect Transistors. *Small* **2015**, *11* (7), 826–833.
(35) Khan, A. H.; Brescia, R.; Polovitsyn, A.; Angeloni, I.; Martín-García, B.; Moreels, I. Near-Infrared Emitting Colloidal PbS Nanoplatelets: Lateral Size Control and Optical Spectroscopy. *Chem. Mater.* **2017**, *29* (7), 2883–2889.
(36) Wang, Y.; Song, Z.; Wan, J.; Betzler, S.; Xie, Y.; Ophus, C.; Bustillo, K. C.; Ercius, P.; Wang, L.-W.; Zheng, H. Strong Structural and Electronic Coupling in Metavalent PbS Moiré Superlattices. *J. Am. Chem. Soc.* **2022**, *144* (51), 23474–23482.
(37) Carr, S.; Fang, S.; Kaxiras, E. Electronic-Structure Methods for Twisted Moiré Layers. *Nat Rev Mater* **2020**, *5* (10), 748–763.
(38) Krauss, T. D.; Wise, F. W. Coherent Acoustic Phonons in a Semiconductor

Quantum Dot. *Phys. Rev. Lett.* **1997**, *79* (25), 5102–5105.
(39) Cui, J.; Beyler, A. P.; Coropceanu, I.; Cleary, L.; Avila, T. R.; Chen, Y.; Cordero, J. M.; Heathcote, S. L.; Harris, D. K.; Chen, O.; Cao, J.; Bawendi, M. G. Evolution of the Single-Nanocrystal Photoluminescence Linewidth with Size and Shell: Implications for Exciton–Phonon Coupling and the Optimization of Spectral Linewidths. *Nano Lett.* **2016**, *16* (1), 289–296.
(40) Hinterding, S. O. M.; Salzmann, B. B. V.; Vonk, S. J. W.; Vanmaekelbergh, D.; Weckhuysen, B. M.; Hutter, E. M.; Rabouw, F. T. Single Trap States in Single CdSe Nanoplatelets. *ACS Nano* **2021**, *15* (4), 7216–7225.
(41) Goupalov, S. V. Low-Frequency Vibrations of Semiconductor Nanoplatelets. *J. Phys. Chem. C* **2019**, *123* (18), 11926–11932.
(42) Girard, A.; Saviot, L.; Pedetti, S.; Tessier, M. D.; Margueritat, J.; Gehan, H.; Mahler, B.; Dubertret, B.; Mermet, A. The Mass Load Effect on the Resonant Acoustic Frequencies of Colloidal Semiconductor Nanoplatelets. *Nanoscale* **2016**, *8* (27),
(43) Fernée, M. J.; Littleton, B. N.; Cooper, S.; Rubinsztein-Dunlop, H.; Gómez, D. E.; Mulvaney, P. Acoustic Phonon Contributions to the Emission Spectrum of Single CdSe Nanocrystals. *J. Phys. Chem. C* **2008**, *112* (6), 1878–1884.
(44) Brodu, A.; Chandrasekaran, V.; Scarpelli, L.; Buhot, J.; Masia, F.; Ballottin, M. V.; Severijnen, M.; Tessier, M. D.; Dupont, D.; Rabouw, F. T.; Christianen, P. C. M.; De Mello Donega, C.; Vanmaekelbergh, D.; Langbein, W.; Hens, Z. Fine Structure of Nearly Isotropic Bright Excitons in InP/ZnSe Colloidal Quantum Dots. *J. Phys. Chem. Lett.* **2019**, *10* (18), 5468–5475.
(45) Clark, S. W.; Harbold, J. M.; Wise, F. W. Resonant Energy Transfer in PbS Quantum Dots. *J. Phys. Chem. C* **2007**, *111* (20), 7302–7305..
(46) Moreels, I.; Lambert, K.; Smeets, D.; De Muynck, D.; Nollet, T.; Martins, J. C.; Vanhaecke, F.; Vantomme, A.; Delerue, C.; Allan, G.; Hens, Z. Size-Dependent Optical Properties of Colloidal PbS Quantum Dots. *ACS Nano* **2009**, *3* (10), 3023–3030.
(47) Califano, M.; Franceschetti, A.; Zunger, A. Temperature Dependence of Excitonic Radiative Decay in CdSe Quantum Dots: The Role of Surface Hole Traps. *Nano Lett.* **2005**, *5* (12), 2360–2364.
(48) Shirazi, R.; Kopylov, O.; Kovacs, A.; Kardynał, B. E. Temperature Dependent Recombination Dynamics in InP/ZnS Colloidal Nanocrystals. *Appl. Phys. Lett.* **2012**, *101* (9), 091910.
(49) Abbarchi, M.; Mastrandrea, C.; Kuroda, T.; Mano, T.; Vinattieri, A.; Sakoda, K.; Gurioli, M. Poissonian Statistics of Excitonic Complexes in Quantum Dots. *Journal of Applied Physics* **2009**, *106* (5), 053504.
(50) Schmidt, T.; Lischka, K.; Zulehner, W. Excitation-Power Dependence of the near-Band-Edge Photoluminescence of Semiconductors. *Phys. Rev. B* **1992**, *45* (16), 8989–8994.
(51) Califano, M.; Franceschetti, A.; Zunger, A. Lifetime and Polarization of the Radiative Decay of Excitons, Biexcitons, and Trions in CdSe Nanocrystal Quantum Dots. *Phys. Rev. B* **2007**, *75* (11), 115401.
(52) Shornikova, E. V.; Yakovlev, D. R.; Biadala, L.; Crooker, S. A.; Belykh, V. V.; Kochiev, M. V.; Kuntzmann, A.; Nasilowski, M.; Dubertret, B.; Bayer, M. Negatively

Charged Excitons in CdSe Nanoplatelets. *Nano Lett.* **2020**, *20* (2), 1370–1377.
(53) Li, H.; Zhitomirsky, D.; Grossman, J. C. Tunable and Energetically Robust PbS Nanoplatelets for Optoelectronic Applications. *Chem. Mater.* **2016**, *28* (6), 1888–1896.
(54) Fernée, M. J.; Plakhotnik, T.; Louyer, Y.; Littleton, B. N.; Potzner, C.; Tamarat, P.; Mulvaney, P.; Lounis, B. Spontaneous Spectral Diffusion in CdSe Quantum Dots. *J. Phys. Chem. Lett.* **2012**, *3* (12), 1716–1720.